

This is a repository copy of *Phenolic Polymers as Model Melanins*.

White Rose Research Online URL for this paper:

<https://eprints.whiterose.ac.uk/id/eprint/200366/>

Version: Published Version

---

## Article:

Galeb, Hanaa A., Eichhorn, Jonas, Harley, Sam et al. (14 more authors) (2023) Phenolic Polymers as Model Melanins. *Macromolecular Chemistry and Physics*. 2300025. ISSN: 1521-3935

<https://doi.org/10.1002/macp.202300025>

---

## Reuse

This article is distributed under the terms of the Creative Commons Attribution (CC BY) licence. This licence allows you to distribute, remix, tweak, and build upon the work, even commercially, as long as you credit the authors for the original work. More information and the full terms of the licence here:

<https://creativecommons.org/licenses/>

## Takedown

If you consider content in White Rose Research Online to be in breach of UK law, please notify us by emailing [eprints@whiterose.ac.uk](mailto:eprints@whiterose.ac.uk) including the URL of the record and the reason for the withdrawal request.

# Phenolic Polymers as Model Melanins

Hanaa A. Galeb, Jonas Eichhorn, Sam Harley, Alexander J. Robson, Laurine Martocq, Steven J. Nicholson, Mark D. Ashton, Hend A. M. Abdelmohsen, Emel Pelit, Sara J. Baldock, Nathan R. Halcovitch, Benjamin J. Robinson,\* Felix H. Schacher,\* Victor Chechik,\* Koen Vercruysse,\* Adam M. Taylor,\* and John G. Hardy\*

Melanins are a class of conjugated biopolymers with varying compositions and functions, which have a variety of potential medical and technical applications. Here, this work examines the conjugated polymers derived from a variety of phenolic monomers (catechol (CAT), levodopa (DOPA), and homogentisic acid (HGA)), using a selection of different analytical chemistry techniques to compare their properties with a view to understanding structure–function relations. The polymers display measurable conductivity, with electronic properties tuned by the functional groups pendant on the polymer backbones (which served as dopants) suggesting their potential for application in electronic devices.

## 1. Introduction

Melanins are a ubiquitous class of biopolymers<sup>[1]</sup> that form colored pigments.<sup>[2]</sup> Their heterogeneous chemical structures and physical properties,<sup>[3,4]</sup> and the conjugation of their backbones result in interesting electronic/optical properties which are of interest to researchers in academia and industry<sup>[5–7]</sup> due to their potential technical<sup>[7,8]</sup> and medical applications.<sup>[9–11]</sup>

In human (and other animal species') physiology two distinct types of melanins are responsible for the coloration of the skin and hair, namely eumelanin and

H. A. Galeb  
Department of Chemistry, Science and Arts College, Rabigh Campus  
King Abdulaziz University  
Jeddah 21577, Saudi Arabia

H. A. Galeb, A. J. Robson, S. J. Nicholson, M. D. Ashton,  
H. A. M. Abdelmohsen, E. Pelit, S. J. Baldock, N. R. Halcovitch,  
J. G. Hardy

Department of Chemistry  
Lancaster University  
Lancaster LA1 4YB, UK  
E-mail: j.g.hardy@lancaster.ac.uk

J. Eichhorn, F. H. Schacher  
Institute for Organic and Macromolecular Chemistry  
Friedrich Schiller University Jena  
Lessingstraße 8, 07743 Jena, Germany  
E-mail: felix.schacher@uni-jena.de

S. Harley, L. Martocq, B. J. Robinson  
Department of Physics  
Lancaster University  
Lancaster LA1 4YW, UK  
E-mail: b.j.robinson@lancaster.ac.uk

H. A. M. Abdelmohsen  
Department of Pharmaceutics and Industrial Pharmacy, Faculty of  
Pharmacy  
Ain Shams University

Abbassia  
African Union Organization Street, Cairo 11566, Egypt  
E. Pelit

Department of Chemistry, Faculty of Art and Sciences  
Kirkklareli University  
Kayali Campus, Kirkklareli 39100, Turkey


B. J. Robinson, J. G. Hardy  
Materials Science Lancaster  
Lancaster University  
Lancaster LA1 4YW, UK

F. H. Schacher  
Jena Center for Soft Matter (JCSM)  
Friedrich Schiller University Jena  
Philosophenweg 7, D-07743 Jena, Germany

V. Chechik  
Department of Chemistry  
University of York  
Heslington, York YO10 5DD, UK  
E-mail: victor.chechik@york.ac.uk

K. Vercruysse  
Department of Chemistry  
Tennessee State University  
Nashville, TN 37209, USA  
E-mail: kvercruysse@tnstate.edu

A. M. Taylor  
Lancaster Medical School  
Lancaster University  
Lancaster LA1 4YW, UK  
E-mail: a.m.taylor@lancaster.ac.uk

 The ORCID identification number(s) for the author(s) of this article can be found under <https://doi.org/10.1002/macp.202300025>

© 2023 The Authors. Macromolecular Chemistry and Physics published by Wiley-VCH GmbH. This is an open access article under the terms of the Creative Commons Attribution License, which permits use, distribution and reproduction in any medium, provided the original work is properly cited.

DOI: 10.1002/macp.202300025

pheomelanin.<sup>[12,13]</sup> Eumelanin is typically described as a brown to black colored material built from DOPA as the precursor, and pheomelanin is typically described as a yellow to red pigment built from a combination of DOPA and the amino acid cysteine.<sup>[14]</sup> The biochemical pathways that lead to these two different classes of melanin are described by the classic Raper–Mason scheme.<sup>[15,16]</sup> In this scheme, DOPA undergoes oxidation and cyclization to intermediates such as 5,6-dihydroxyindole and 5,6-dihydroxyindole-2-carboxylic acid which then polymerizes yielding eumelanin. In the presence of cysteine, this pathway is diverted to a different set of intermediates, e.g., 5-S-cysteinyl-DOPA, 1,4-benzothiazine, or 1,4-benzothiazine-3-carboxylic acid, the polymerization of which produces pheomelanin.<sup>[14,17–19]</sup> In human skin melanins are produced in specialized cells, the melanocytes, inside specialized organelles, melanosomes, wherein melanins are deposited using the melanocyte protein PMEL (also known as premelanosome protein),<sup>[20,21]</sup> these melanosomes are shed off as extracellular vesicles and taken up by keratinocytes where melanin is dispersed in the cytosol or may be shed from keratinocytes inside exosomes.<sup>[22]</sup> Another type of melanin found in human physiology is neuromelanin built from dopamine with or without the presence of cysteine. Neuromelanin is primarily produced in the substantia nigra and locus coeruleus and accumulates with age. Both these regions of the brain are targeted in Parkinson's disease and the locus coeruleus is targeted in Alzheimer's disease. As a consequence, the possible protective or toxic functions of neuromelanin are extensively studied.<sup>[23]</sup> Neuromelanin is synthesized using a variety of proteins as templates and are accumulated inside autophagosomes which fuse with lysosomes to produce an autolysosome. Ultimately these organelles will contain materials with neuromelanin bound to protein and to lipid materials; primarily dolichols and dolicholic acids. The nature of these interactions or bonds currently being unknown.<sup>[23]</sup> Upon the death of neuromelanin-containing neurons, the neuromelanin material is released in the extracellular environment where it may activate microglia.<sup>[24]</sup>

In the fungal species *Cryptococcus neoformans* melanin is found in the organism's cell wall, covalently bound to chitin or strongly associated with other polysaccharides like chitosan or plasma membrane-derived lipids.<sup>[25]</sup> The polysaccharides are used as scaffolds for melanin synthesis as the pigment is not retained in the cell wall in the absence of these polysaccharides; observed in the so-called leaky-melanin phenotypes. Apart from fungi other microorganisms, yeasts, actinomycetes, or bacteria, produce melanin-like materials which are often excreted into the extracellular environment and readily isolated.<sup>[26]</sup> Plant-based melanins tend to be brown-to-black pigments commonly found in seeds but typically devoid of nitrogen.<sup>[27]</sup> Apart from their presence in seeds, melanin synthesis in plants is also associated with the browning reactions that occur in damaged tissues. Although melanin in seeds is found extracellularly and may be associated with a polyvinyl aromatic alcohol substance, termed phytomelanin, melanins may be produced intracellularly and stored in melanoplasts.<sup>[27]</sup>

Many potential purposes or functions of melanins in the extracellular environment have been suggested and its extracellular presence could have beneficial or detrimental consequences.<sup>[23,28]</sup> Melanins can adhere to a wide variety of

biomolecules found in the biological milieu, with important biologically relevant roles<sup>[29–31]</sup>; and this has inspired the investigation of the interactions of melanins and other materials by fundamental and application-oriented researchers in academia and industry.<sup>[5,32–36]</sup>

Phenolic monomers are common building blocks of melanins (observed in allomelanin, eumelanin, neuromelanin, pheomelanin, and pyromelanin),<sup>[37]</sup> and are known to play important roles in intermolecular/material interactions,<sup>[38–40]</sup> and here we examine the conjugated polymers derived from a variety of phenolic monomers (CAT, DOPA, and HGA) to understand the role of functional groups pendant on the polymer backbones on their optoelectronic properties.<sup>[41]</sup> A selection of different analytical techniques are employed for these studies, including: UV–Vis spectroscopy, nuclear magnetic resonance (NMR) spectroscopy, X-ray diffraction (XRD), differential scanning calorimetry (DSC), X-ray photoelectron spectroscopy (XPS), zeta potential measurements, transmission electron microscopy (TEM), scanning electron microscopy (SEM), energy dispersive X-ray (EDX) spectroscopy, Fourier-transform infrared (FTIR) spectroscopy, electron paramagnetic resonance (EPR) spectroscopy, cyclic voltammetry (CV), and conductivity measurements. The properties of the conjugated polymers suggests they may find application in electronic devices.

## 2. Results and Discussion

Various methods of polymerization of aromatics (e.g., phenols) exist, including enzymatic,<sup>[42–47]</sup> electrochemical,<sup>[48–57]</sup> oxidative,<sup>[58,59]</sup> etc. and the polymerization of phenols is the subject of an excellent review from Kobayashi and co-workers,<sup>[58,59]</sup> which examined the propensity for C–C or C–O–C bond formation which would be expected to play a role in the conductivity of the resulting polymers (polymers connected via C–C bonds akin to graphene derivatives<sup>[60]</sup> are expected to have higher electrical conductivity than polymers connected via C–O–C bonds). A study from Nishide and co-workers mixing phenol with an oxidant (potassium ferricyanide) under basic conditions in water (pH > 13.5) yielded a mixture of poly(phenyleneoxide)s, where the constituent monomers were connected either via C–O–C (Ar–O–Ar, aromatic ether) or C–C (Ar–Ar) bonds.<sup>[61]</sup> C–O–C bonds can also form via the combination of two free phenoxy radicals or indeed via an enzyme mediated pathway and the products tend to be complex mixtures including products wherein the monomers are connected by C–C bonds too.<sup>[58]</sup>

Indeed, in a previous study we investigated the polymerization of HGA under various conditions in vitro, specifically in the absence (control) or presence of enzymes (a laccase, peroxidase, or tyrosinase) at either pH 5 or 7.4 with a view to understand the potential role of enzymes and pH on the formation of ochronotic pigment: we observed interesting trends in the yields of poly-HGAs produced with subtle differences in their properties; notably, conductive tip atomic force microscopy data for polyHGAs showed that those generated in the presence of LACC at pH 7.4, or HRP at pH 7.4 or 5.0, respectively, displayed measurable conductivity owing to the formation of polymers connected via C–C bonds.<sup>[47]</sup>

In this study, a green approach was applied using a weakly basic aqueous solution of the commercially available monomers

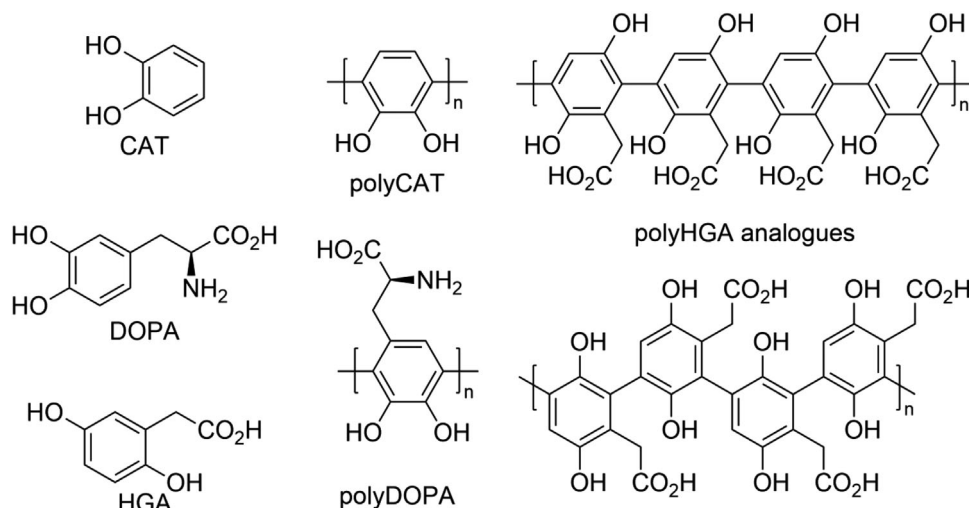


**Figure 1.** Structures of the monomers (catechol (CAT), levodopa (DOPA), or homogentisic acid (HGA)) used to form model melanins (polyCAT, polyDOPA, or polyHGA, respectively) that are studied herein.

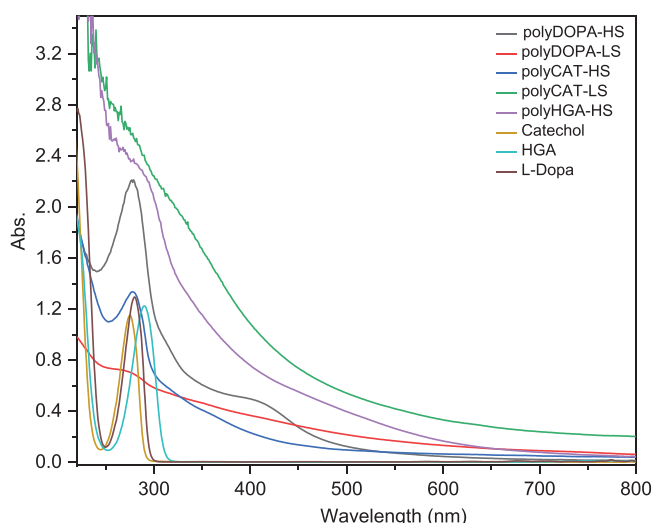


**Figure 2.** UV-Vis spectra of the polymers studied herein.

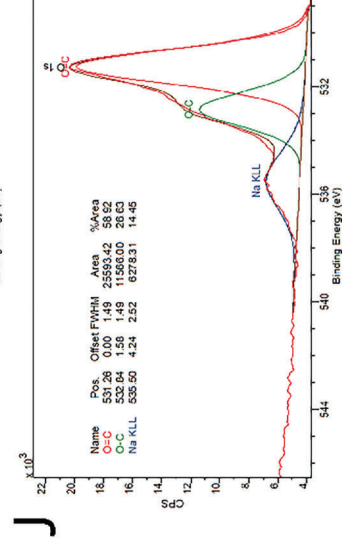
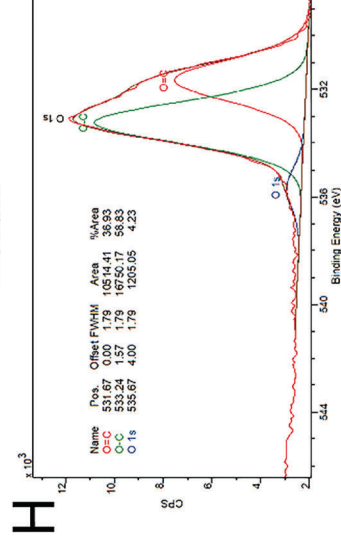
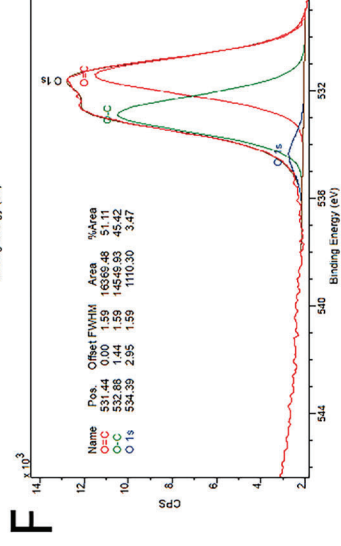
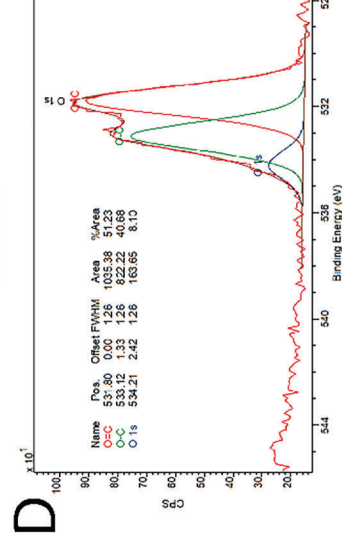
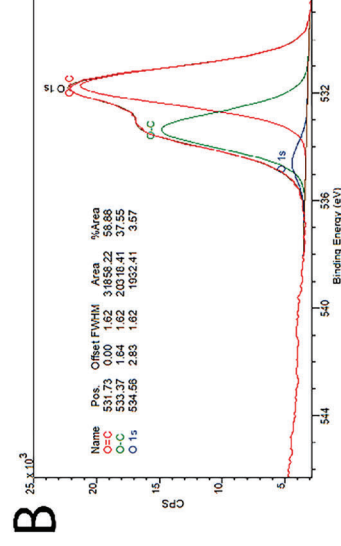
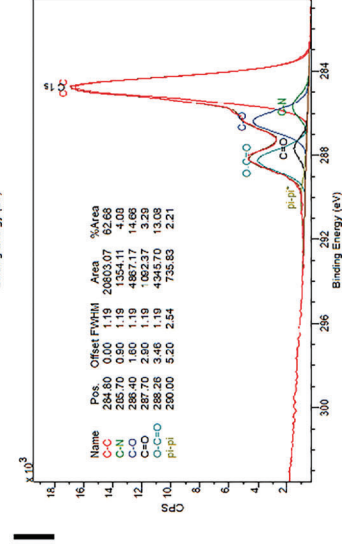
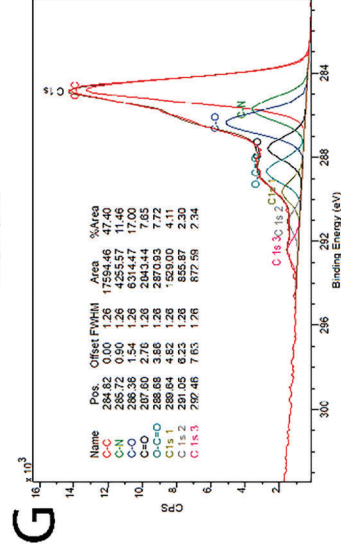
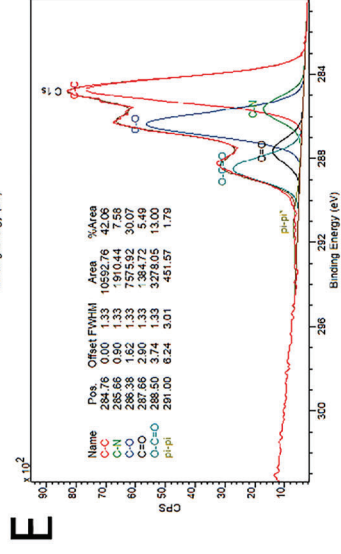
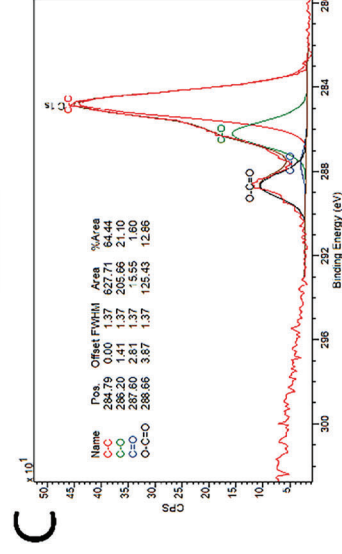
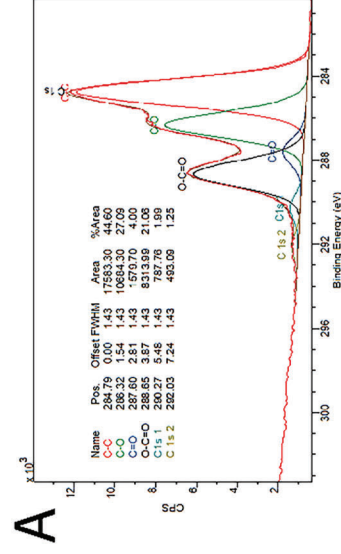
CAT, DOPA, and HGA (**Figure 1**) to polymerize the monomers via autooxidation with a view to understand the potential role of subtle differences in monomer structure and the properties of the resulting conjugated polymers, polyCAT, polyDOPA, and polyHGA, respectively (Schemes S1–S3, Supporting Information).

The polymerizations of CAT and DOPA resulted in the formation of a colored precipitate (isolated by centrifugation and washing) termed the insoluble or low solubility fraction (polyCAT-LS or polyDOPA-LS, respectively), and supernatant (that was dialyzed against DI water and lyophilized) termed the high solubility fraction (polyCAT-HS or polyDOPA-HS, respectively); and under the polymerization conditions used the polymerization of HGA resulted in the production of only a high solubility fraction (polyHGA-HS). The polymers showed a broad absorption typical of melanins in the UV-Vis spectra (**Figure 2**), which are also suggestive of various oxidation states of the monomeric units consti-

tuting the backbone of the polyCAT-HS, polyCAT-LS, polyDOPA-HS, polyDOPA-LS, and polyHGA-HS, respectively.

The  $^1\text{H}$  NMR spectra recorded in  $\text{D}_2\text{O}$  of the monomers CAT, DOPA, and HGA show sharp peaks characteristic of low molecular weight species (Figures S1–S3, Supporting Information, respectively), whereas the  $^1\text{H}$  NMR spectra of the polymers (polyCAT-HS, polyCAT-LS, polyDOPA-HS, polyDOPA-LS, and polyHGA-HS) are markedly different. The  $^1\text{H}$  NMR spectra of the soluble fractions (polyCAT-HS, polyDOPA-HS, and polyHGA-HS) have some sharp peaks (due to the pendant functional groups) and broad lines characteristic of high molecular weight species, and the  $^1\text{H}$  NMR spectra of the low solubility fractions (polyCAT-LS, polyDOPA-LS) are broader still characteristic of high molecular weight species and/or aggregation of the oligomers/polymers that is characteristic of polyphenols<sup>[62]</sup> and melanins more generally, leading to relatively featureless solid-like spectra (Figures S1–S3, Supporting Information). XRD patterns of the samples suggested they were largely amorphous, confirmed by the very broad peak at  $2\theta = 15\text{--}40^\circ$  (Figure S4, Supporting Information), characteristic of natural and synthetic melanins.<sup>[63–66]</sup> DSC data (Figures S5–S9, Supporting Information) showed endothermic peaks attributed to the presence of water as previously reported for melanins,<sup>[67]</sup> but were otherwise structurally uninformative due to their amorphous nature.

XPS data (**Figure 3** and Figure S10, Supporting Information) confirmed the polymer powders were predominantly composed of C and O (with traces of N from the  $\text{NH}_2$  in polyDOPA-HS and polyDOPA-LS, Na/Ca/F [residual buffer/Kapton tape] and Si [potentially from underlying substrate]). The C 1s spectra confirmed the presence of a number of clear peaks, which we correlate to common carbon binding environments (C–C/H, C–N, C–O, C=O, O–C=O).<sup>[68]</sup> Small peaks towards the higher binding energy side of the C1s spectra may be indicative of  $\pi\text{--}\pi^*$  shake-up features. The fluorine signal evident in the wide scan for polyDOPA-LS may also contribute to the higher energy peaks in the corresponding C 1s spectra.<sup>[68]</sup> O 1s spectra are fitted with two major peaks which are expected to correspond to O=C and O–C bonds in agreement with the C 1s spectra, though some





minor peaks are also required to fit the spectra potentially indicating a range of different oxidation states. A Na KLL Auger peak at  $\approx 536$  eV is also evident in the O1s spectra for polyHGA-HS, correlating with the strong Na signal noted in the wide-scan for this polymer. We note that there are clear differences between the polymers, in particular the varying levels of C–O and C=O bonds (plausibly due to both quinones present in all polymers and carboxylic acids in polyDOPA-LS, polyDOPA-HS, and polyHGA-HS, respectively) suggestive of differing oxidation states for the monomers incorporated in the backbone of the polymers. For polyDOPA-HS and polyDOPA-LS nitrogen N 1s (Figure S10, Supporting Information) is dominated by a peak at c. 400 eV (likely corresponding to the amine in DOPA), and a smaller peak at c. 402 eV (likely corresponding to protonated amine groups, e.g.,  $\text{NH}_3^+$ ).<sup>[69]</sup>

Zeta potential measurements indicate all of the polymers/particles are anionic due to deprotonation of phenols and carboxylic acids (polyDOPA-LS, polyDOPA-HS, and polyHGA-HS); the zeta potentials for the polyCAT-HS ( $-9.83 \pm 0.84$ ) and polyCAT-LS ( $-17.83 \pm 0.75$ ) are somewhat lower than those of phenol, amine and carboxylic acid containing polyDOPA-HS ( $-15.63 \pm 1.25$ ) and polyDOPA-LS ( $-33.03 \pm 0.12$ ), and phenol and carboxylic acid containing polyHGA-HS ( $-37.00 \pm 3.30$ ). The interaction of cationic amines with the anionic phenols and carboxylic acids presents in polyDOPA account for the lower zeta potentials for polyDOPA than amine-free polyHGA, and the higher zeta potentials for the LS products than HS products suggest the hydrophobic parts of the polymers are buried within the particles with hydrophilic functional groups clustered on the particles' surfaces as the polymers constituting them assemble/aggregate.<sup>[70]</sup>

TEM, SEM, and EDX were used to study the morphology and elemental composition of the of the HS and LS polymer fractions produced. TEM of dilute solutions of the polymers deposited on TEM grids showed the presence of nanoscale particles of 10–100 nm characteristic of melanins (the formation of which is proposed to proceed via a nucleation and growth mechanism) (Figure 4).<sup>[6,70]</sup> SEM images of lyophilized solutions of the polymers deposited on SEM stubs shows the particles/precipitates formed were irregularly shaped with sizes between tens to hundreds of micrometers characteristic of melanins (Figure 4); while the HS particles are generally smaller than the LS precipitates, there is no meaningful correlation between particle/precipitate shapes/sizes as the polymers are produced under unconstrained conditions.<sup>[47]</sup> By comparison, the shapes/sizes of melanin particles/precipitates in vivo would be constrained by the intracellular/extracellular environment in which they are produced. EDX data suggests that all samples are mainly composed of C and O for all polymers with a trace of N present in the polyDOPA samples (similar to the XPS data), with additional traces of Ca, K, and Na from the buffer, Au (sputter coating) and Si (substrate) (Figure 4 and Figure S11, Supporting Information). Interestingly, EDX data shows that the polymers in the highly soluble fractions have higher metal ion contents (measured as relative

abundance by EDX) than the low solubility fractions, polyCAT-HS (Ca:  $8.9\% \pm 0.1\%$ ; Na:  $0.4\% \pm 0.1\%$ ), polyDOPA-HS (Ca:  $8.4\% \pm 0.1\%$ ; Na:  $1.6\% \pm 0.9\%$ ), polyHGA-HS (Ca:  $0.3\% \pm 0.1\%$ ; Na:  $15.3\% \pm 0.8\%$ ), by comparison with polyCAT-LS (Ca:  $2.1\% \pm 0.4\%$ ; Na:  $0.1\% \pm 0.1\%$ ) and polyDOPA-LS (Ca:  $0.2\% \pm 0.1\%$ ; Na:  $0.0\% \pm 0.0\%$ ), confirming the polyphenol's ability to bind metal ions,<sup>[71,72]</sup> a putative role for melanins in biology<sup>[56,73]</sup> and underpinning their application in energy storage.<sup>[74–77]</sup>

FTIR spectroscopy was used to analyze the polymers produced, all of which were broader than for their constituent monomers as expected for polymeric species with a variety of chemical environments (Figure 5, Figure S12, Supporting Information), characteristic of natural and synthetic melanins.<sup>[78]</sup> A discernible difference in the FTIR spectra of all polymers was the broadening/diminution of peaks at  $\approx 970$   $\text{cm}^{-1}$  from the aromatic hydrogens suggestive of C–C bond formation during polymerization, with broadening of bands at  $1500\text{--}1520$   $\text{cm}^{-1}$  (aromatic C=C bonds) and the weak band at  $\approx 1580$   $\text{cm}^{-1}$  (aromatic C=C). Peaks at  $\approx 1200\text{--}1210$   $\text{cm}^{-1}$  corresponding to phenolic OH.<sup>[43,44,79]</sup> The broad bands at  $\approx 3000$   $\text{cm}^{-1}$  attributed to aromatic C–H, and at  $3400\text{--}3200$   $\text{cm}^{-1}$  attributed to stretching vibrations of the OH in all polymers and  $\text{NH}_2$  in polyDOPAs.<sup>[80–83]</sup>

Melanins display paramagnetic character due to free radicals in their structures (e.g., semiquinone free radicals) which absorb microwaves under magnetic fields yielding spectra characteristic of the radical species present, consequently EPR spectroscopy was used to study the powders. X-band EPR spectra of all polymer powders showed single peak centered around  $g = 2.0023\text{--}2.005$ , with peak-to-peak width  $\approx 4\text{--}5$  G, typical of melanin pigments (Figure 6).<sup>[5]</sup>

Low solubility fractions polyCAT-LS and polyDOPA-LS were dominated by the signal of a carbon centered radical ( $g = 2.0033$ ), typical of eumelanins. PolyHGA-HS sample also showed a similar spectrum albeit at a slightly higher  $g$  value (2.0036). Interestingly, the two other high-solubility melanins polyCAT-HS and polyDOPA-HS showed clearly asymmetrical spectra with a high contribution of the semiquinone radical (Figure 7) which is probably due to complexation with  $\text{Ca(II)}$ <sup>[84,85]</sup> which is present in these two materials only (see EDX data above).

Cyclic voltammetry can be used to study the reduction/oxidation processes and electron transfer properties of polyphenols such as those studied herein (voltammograms for CAT and polyCATs are shown in in Figure S13 (Supporting Information), for DOPA and polyDOPA in Figure S14 (Supporting Information), and for HGA and polyHGA in Figure S15, Supporting Information). The cyclic voltammograms of the polymers generated in this study at pH 5 typically show anodic peaks at  $\approx 0.15\text{--}0.4$  V and the corresponding cathodic peaks at  $\approx -0.2\text{--}0$  V versus Ag/AgCl (reference electrode), whereas, at pH 7.4 the oxidation and reduction peaks were less well resolved, i.e., the polymers were electroactive in acidic medium while electroinactive in neutral medium. This is consistent with the literature for polyCATs,<sup>[44]</sup> polyDOPAs,<sup>[86]</sup> and polyHGAs,<sup>[47]</sup>

**Figure 3.** X-ray photoelectron spectroscopy (XPS) spectra. A) polyCAT-HS C 1s core line spectra. B) polyCAT-HS O 1s core line spectra. C) polyCAT-LS C 1s core line spectra. D) polyCAT-LS O 1s core line spectra. E) polyDOPA-HS C 1s core line spectra. F) polyDOPA-HS O 1s core line spectra. G) polyDOPA-LS C 1s core line spectra. H) polyDOPA-LS O 1s core line spectra. I) polyHGA-HS C 1s core line spectra. J) polyHGA-HS O 1s core line spectra.

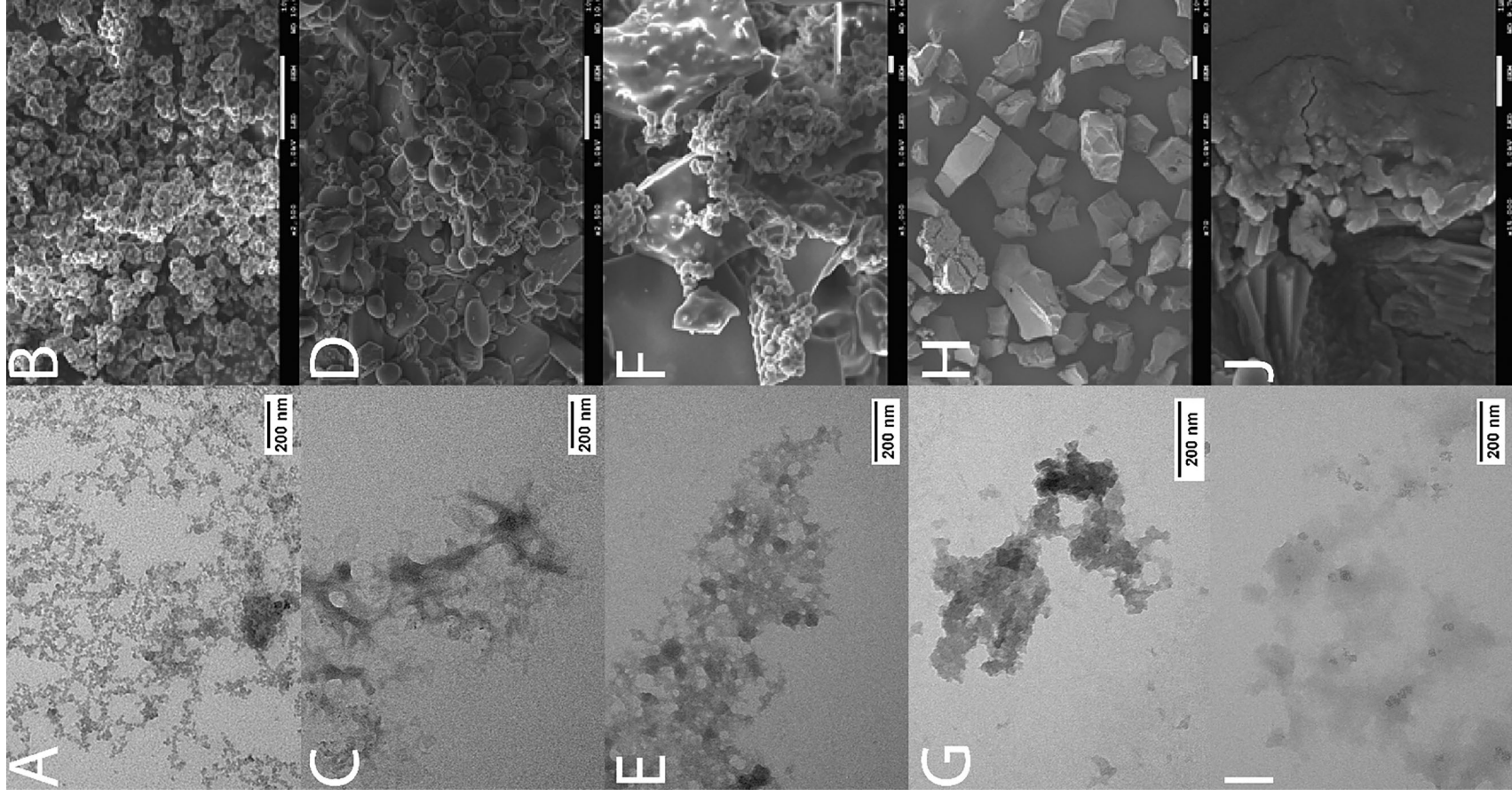


**Figure 4.** Transmission electron microscopy (TEM) and scanning electron microscopy (SEM) images of samples studied herein. A) polyCAT-HS TEM. B) polyCAT-HS SEM (scale bar represents 10  $\mu\text{m}$ ). C) polyCAT-LS TEM. D) polyCAT-LS SEM (scale bar represents 10  $\mu\text{m}$ ). E) polyDOPA-HS TEM. F) polyDOPA-HS SEM (scale bar represents 1  $\mu\text{m}$ ). G) polyDOPA-LS TEM. H) polyDOPA-LS SEM (scale bar represents 1  $\mu\text{m}$ ). I) polyHGA-HS TEM. J) polyHGA-HS SEM (scale bar represents 1  $\mu\text{m}$ ).

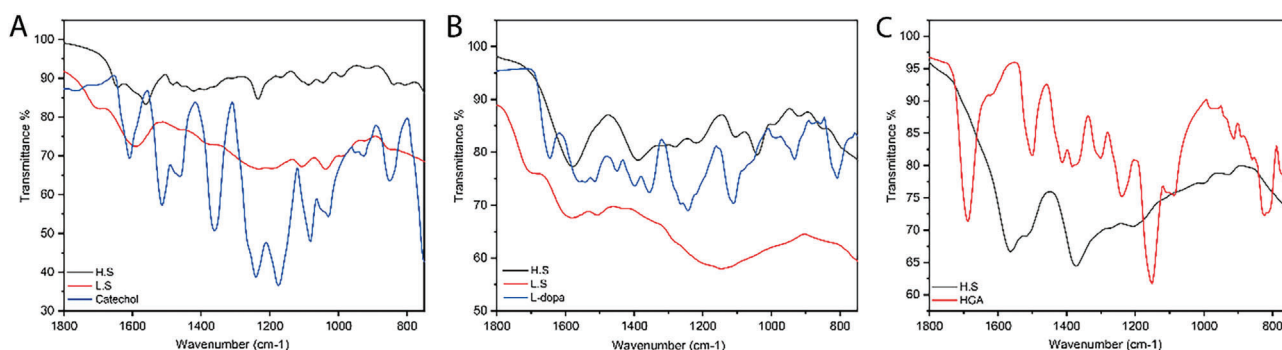


**Figure 5.** Fourier-transform infrared (FTIR) spectra of monomers and polymers. A) Catechol (CAT), polyCAT-HS, and polyCAT-LS. B) levodopa (DOPA), polyDOPA-HS, and polyDOPA-LS. C) Homogentisic acid (HGA) and polyHGA-HS.

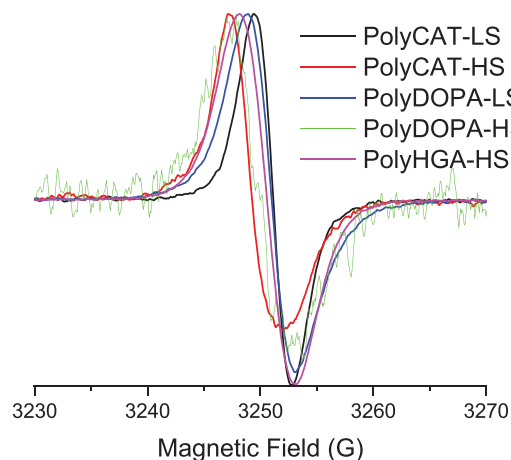


**Figure 6.** X-band electron paramagnetic resonance (EPR) spectra of polymers studied herein.

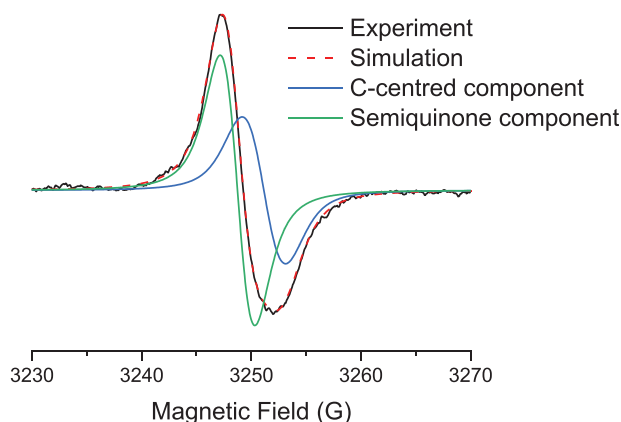


**Figure 7.** Experimental electron paramagnetic resonance (EPR) spectrum of polyCAT-HS (black) and simulation (red). The simulation included a broad C-centered component ( $g = 2.0033$ , 41.6%) and a sharper semiquinone radical ( $g = 2.0048$ , 58.4%).

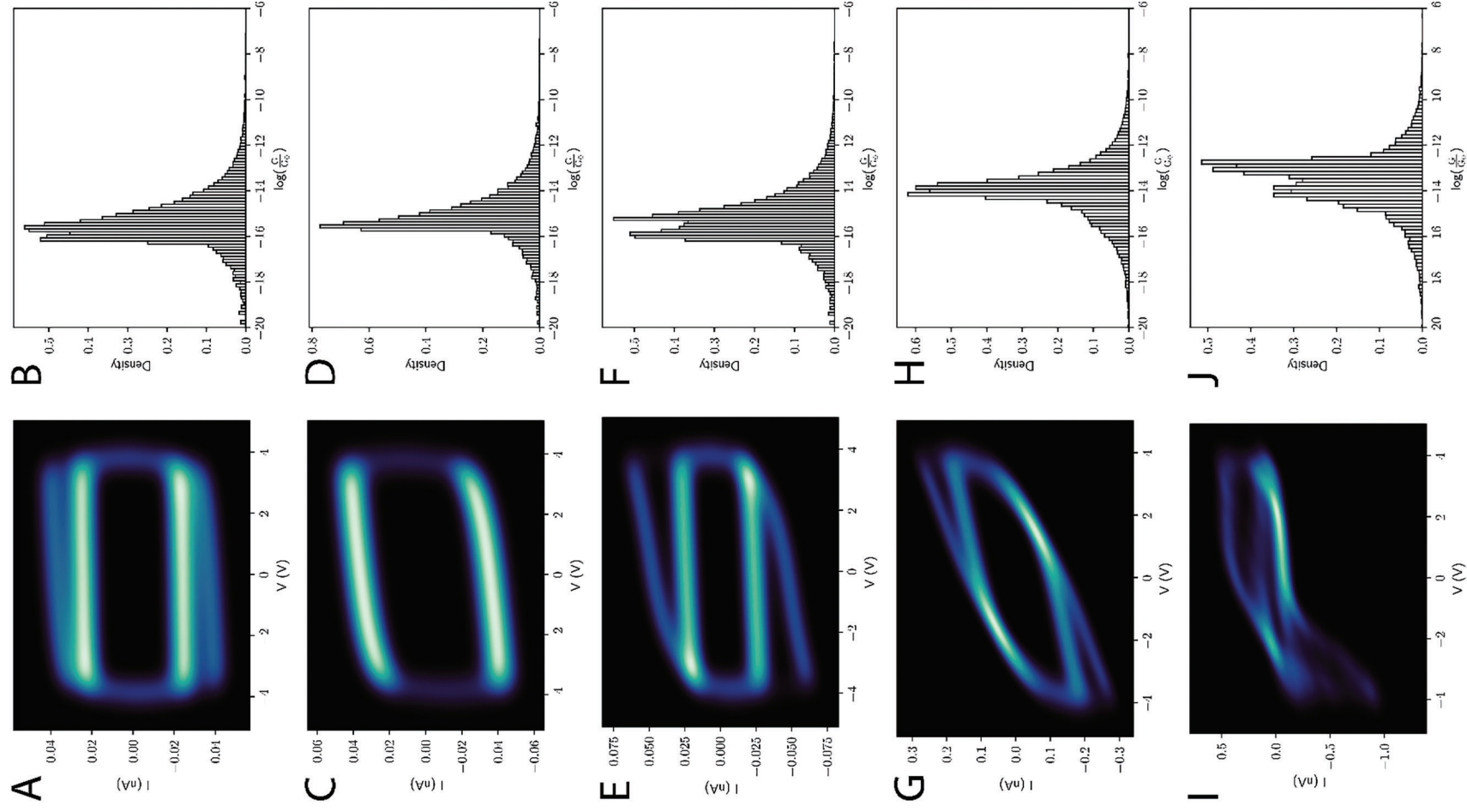
and confirms the role of protons in the electroactivity of the polymers.<sup>[87]</sup> The cyclic voltammograms are consistent after multiple scans demonstrating their stability under the experimental conditions for the duration of the experiment, and their unsymmetrical cathodic and anodic peaks are attributed to the difference in background current and kinetic limitations.<sup>[87]</sup>

There has been significant interest in correlating the structure and electronics properties of melanins,<sup>[87]</sup> and to assess if the electronic properties of the samples studied herein have electronic properties useful for application in electronic devices<sup>[8,88,89]</sup> their conductance was measured. Interestingly, the powders isolated from lyophilised solutions of the polymers showed them to be measurably conductive (**Figure 8**). The polymers had average  $\log_{10} \frac{G}{G_0}$  values of  $-15.4 \pm 1.2$ ,  $-15.1 \pm 1.2$ ,  $-15.3 \pm 1.2$ ,  $-14.0 \pm 1.3$  and  $-13.6 \pm 1.3$ , for polyCAT-HS, polyCAT-LS, polyDOPA-HS, polyDOPA-LS, and polyHGA-HS, respectively. The differences in the electronic properties of the polymers<sup>[41,90,91]</sup> are likely to be related to a subtle combination of the extended conjugation length of the LS polymers produced versus HS polymers; the hierarchical assembly of the polymers (governed by intramolecular and intermolecular interactions)<sup>[70,92]</sup>; and the ability of the anionic component of the polymers to serve as a dopant for the polymers (supported by zeta potential measurements), akin to self-doped conducting polymers.<sup>[93–96]</sup>

### 3. Conclusion

This work follows on from our earlier work that was the first detailed chemical analysis of polyHGA.<sup>[47]</sup> Herein polymerization of a variety of phenolic monomers (CAT, DOPA, and HGA), yielded conjugated polymers polyCAT-HS, polyCAT-LS, polyDOPA-HS, polyDOPA-LS, or polyHGA-HS, respectively. A variety of analytical techniques (UV–Vis, NMR, XRD, DSC, XPS, zeta potential measurements, TEM, SEM, EDX, FTIR, EPR, CV, and conductivity measurements) were employed to examine the polymers produced. TEM and SEM images reported here show the structure of the polyHGA particles that have similarities to those of polyDOPA formed in geometrically unconstrained





conditions. The significance of our findings on HGA and poly-HGA is important for the field of Alkaptonuria, where it has long been discussed that the polymeric material that is accumulated from HGA is a polymer derived from benzoquinone acetic acid.<sup>[97,98]</sup> This has appeared in the literature regarding the disease for many decades, with recent interest and advances in understanding the pathophysiological processes shedding new light on the chemical behavior of HGA in tissues and cells.<sup>[47,99,100]</sup> Understanding the polymerization process offers new therapeutic opportunities to treat early and established polymer pigmentation in connective tissues of patients with this condition. Furthermore, the experiments revealed interesting trends in the properties of the polymers, notably conductivity measurement data for the polymers confirmed they displayed measurable conductivity, with electronic properties tuned by the functional groups pendant on the polymer backbones (which served as dopants) suggesting their potential for application in electronic devices.<sup>[101–106]</sup>

## 4. Experimental Section

**Materials:** Unless otherwise noted, all chemicals and consumables were supplied by Sigma Aldrich (Merck), Gillingham, UK.

**Synthesis of Melanins:** An amount of 300 mg of melanin precursor (catechol (1,2-dihydroxybenzene), CAT; levodopa, DOPA; homogentisic acid, HGA) was dissolved in 50 mL of acetate buffer ( $50 \times 10^{-3}$  M; pH = 6.5) and the reaction was initiated by the addition of 50 mL of  $\text{Na}_2\text{CO}_3$  ( $50 \times 10^{-3}$  M). The mixtures were stirred at room temperature and monitored using chromatography to ensure that the reaction of the melanin precursor compound was complete. In the cases of melanin precursors DOPA and catechol, 10 mL of 0.5 M  $\text{CaCl}_2$  was added to the reaction mixtures; after standing at room temperature overnight a precipitate was observed to have formed, the supernatant was collected after centrifugation (5 min at 4 K rpm) and these were dialyzed against DI water for two days (using dialysis tubes with MWCO of 3.5 kDa) and lyophilized (this is termed the “high solubility fraction”, abbreviated to HS). The precipitates were washed with: a) water, b) 0.1 N HCl and c) water, and lyophilized (this is termed the “low solubility fraction”, abbreviated to LS). For CAT and DOPA a high solubility fraction and a low solubility fraction were obtained, polyCAT-HS, polyCAT-LS, polyDOPA-HS, and polyDOPA-LS, respectively; whereas in the case of HGA it is important to note that only a high solubility fraction was obtained (polyHGA-HS).

**UV–Vis Spectroscopy:** Spectra were recorded in UV Quartz cuvettes (Standard Cell with PTFE Stopper, manufactured in UV Quartz (195 nm–2.5  $\mu\text{m}$ ); path length 10 mm, inside width 10 mm, volume 3.5 mL; outside dimensions (H  $\times$  W  $\times$  D) 45  $\times$  12.5  $\times$  12.5 mm) on an Agilent Technologies Cary 60 UV–Vis supplied by Thermo Fisher Scientific in Heysham, UK. Samples were at a concentration of 0.0026 mg mL<sup>−1</sup> in water.

**Nuclear Magnetic Resonance (NMR) Spectroscopy:** <sup>1</sup>H NMR (400 MHz) spectra were recorded using a Bruker AVANCE III 400 NMR spectrometer using residual solvent as internal standards in deuterated solvents (D<sub>2</sub>O). Chemical shift ( $\delta$ ) values were recorded in parts per million (ppm).

**X-Ray Diffraction (XRD):** XRD patterns were recorded using a Rigaku SmartLab powder diffractometer with a  $2\theta$  scattering range of 10° to 90° and a resolution of 0.1°.

**Differential Scanning Calorimetry (DSC):** Samples were analyzed using a Mettler Toledo STARE Calorimeter using airtight aluminum crucibles under an inert nitrogen atmosphere. Each sample was heated from room

temperature to 150 °C at 10 °C min<sup>−1</sup> increments before being cooled to −55 °C. This cycle was repeated a further two times for each sample.

**X-Ray Photoelectron Spectroscopy (XPS):** A Kratos Analytical Axis Supra X-ray photoelectron spectrometer with a monochromatic Al K $\alpha$  source (1.487 keV) was used to analyze surface chemical composition. Powder samples were mounted using carbon tape in a well-shaped holder. An internal flood gun was applied for neutralizing charging effects. Wide-scan spectra were recorded at a pass energy of 160 eV, a step size of 1 eV, and a sweep time of 120 s. Core line spectra were recorded at a pass energy of 20 eV, a step size of 0.1 eV, and a sweep time of 120 s. Samples were measured in triplicate at a take-off angle of 90° (relative to the surface), power of 225 W (15 kV  $\times$  15 mA) and an analysis area of 700  $\times$  300  $\mu\text{m}$ . Data were quantified and processed by CasaXPS (ver.2.3.23PR 1.0, Casa Software Ltd) using linear baseline correction and Kratos Analytical sensitivity factors. All spectra were adjusted for charge compensation effects by offsetting the binding energy relative to the C–C component of the C 1s spectrum at 284.8 eV.

**$\xi$  Potential Measurement:** Zeta-potentials were measured on a Zeta-Sizer Nano ZS from (Malvern Instruments, Malvern, UK) via M3-PALS technique with a laser beam at 633 nm. The detection angle was 13°. All measurements were performed in three consecutive runs and the values obtained averaged.

**Transmission Electron Microscopy (TEM):** For TEM analysis copper grids were rendered hydrophilic by Ar plasma cleaning for 30 s (Diener Electronics). An amount of 10  $\mu\text{L}$  of the respective sample solution were applied to the grid and excess sample was blotted with a filter paper. TEM images were acquired with a 200 kV FEI Tecnai G2 20 equipped with a 4k  $\times$  4k Eagle HS CCD and a 1k  $\times$  1k Olympus MegaView camera for overview images.

**Scanning Electron Microscopy (SEM):** Prior to imaging the samples were sputter coated with a 10 nm layer of gold. The structures were observed using either a JEOL JSM–6390LV operating at 15 kV or a JEOL JSM 7800F scanning electron microscope (JEOL, Welwyn Garden City, UK) operating at 10–15 kV.

**Energy Dispersive X-Ray (EDX) Spectroscopy:** For qualitative EDX analysis, the samples were sputter coated with a layer of gold (60 s, 20 mA,  $8 \times 10^{-2}$  mBar,  $\approx 5$  nm) using a Quorum Q150RES sputter coater (Quorum Technologies Ltd) and then investigated using a field-emission SEM JEOL JSM 7800F with an EDX system (X-Max50, Oxford Instruments, Abingdon, UK) at 10 mm working distance and 10 kV voltage mounted on a brass JEOL holder with 25 mm carbon tables (G3348N, Agar Scientific, Stansted, UK). Three measurements were performed per sample and average results are presented.

**Fourier-Transform Infrared (FTIR) Spectroscopy:** All spectra were recorded using an Agilent Technologies Cary 630 FTIR instrument (Agilent Technologies Ltd., Cheadle, UK) at a resolution of 1 cm<sup>−1</sup> and was an average of 16 scans.

**Electron Paramagnetic Resonance (EPR) Spectroscopy:** Room temperature EPR spectra of polyHGA powders were recorded at X-band on a JEOL X320 spectrometer using 0.1 mW microwave power and 1 G modulation width (100 kHz modulation frequency). The g values were determined by using Mn<sup>2+</sup> marker. The spectra were simulated using EasySpin toolbox for MatLab.<sup>[107]</sup>

**Cyclic Voltammetry (CV):** Voltammetry was carried out using an EmStat 3+ potentiostat with PSTrace 4.7 software (PalmSens Houten, Netherlands) at ambient temperature. The cell comprised of a three-electrode system with a Ag/AgCl reference electrode, a gold counter electrode and glassy carbon working electrode (GCE). The GCE was coated with a film prepared by drying 10  $\mu\text{L}$  of a suspension of polymer (1 mg) in Nafion perfluorinated resin solution (10  $\mu\text{L}$  of a 5 wt% in mixture of lower aliphatic alcohols and water, contains 45% water; product number 510211 from Sigma Aldrich, Gillingham, UK) overnight in a fume hood at room temperature. Buffer (pH 5 or 7.4, described above) was

**Figure 8.** Conductance data for polymers studied herein. A) polyCAT-HS *I*–*V* curves. B) polyCAT-HS conductance histogram. C) polyCAT-LS *I*–*V* curves. D) polyCAT-LS conductance histogram. E) polyDOPA-HS *I*–*V* curves. F) polyDOPA-HS conductance histogram. G) polyDOPA-LS *I*–*V* curves. H) polyDOPA-LS conductance histogram. I) polyHGA-HS *I*–*V* curves. J) polyHGA-HS conductance histogram.

used as the electrolyte, with a scan rate of  $0.01 \text{ V s}^{-1}$  between  $-1$  to  $1 \text{ V}$ .

**Conductance Measurements:** The setup used is depicted in Figure S16 (Supporting Information). Samples were mounted onto a polished copper disc using adhesive double sided copper tape, with silver paint covering one corner. This was installed on an electrically insulating stage inside a Bruker multimode AFM. A function generator (RS Pro RSDG800, RS calibrated, 14-bit) was used to apply a varying bias voltage to the sample ( $8 \text{ V}$  peak to peak  $4 \text{ Hz}$  triangle wave). A conductive probe made from  $0.25 \text{ mm}$  diameter gold wire ( $99.9\%$ , hard, Goodfellow) cut to a sharp point was installed in the conductive probe holder of the AFM, such that the coarse approach  $z$  motor could be used to control the probe-sample separation. The current flowing from sample to probe was amplified by a  $10^9 \text{ VA}^{-1}$  gain transimpedance amplifier (FEMTO DLPCA-200, FEMTO Messtechnik GmbH, Berlin, Germany). The applied bias and resulting current were digitised and recorded simultaneously using the analog inputs of the Bruker Nanoscope V SPM controller.

The probe and sample were slowly brought into contact using the  $z$  stepper motor of the AFM, with feedback disengaged. The measured current amplitude increased from  $\approx 0 \text{ nA}$  when not in contact to a stable non-zero value once contact was established. Further advancing the probe into the sample did not change the current amplitude until the probe pushed all the way through to the copper tape underneath, at which point a very large conductance ( $\approx$ several  $\text{mS}$ ) was measured. This showed that the contact force between the sample and probe did not have a significant effect on the measurements. Once contact was established, 3072 full waveforms were measured. This was repeated for three different positions on the sample to account for variations in sample thickness, contact geometry and engagement force.  $I$ - $V$  curves were produced from the aggregate data using kernel density estimation to plot the density distribution of all the measurements. Conductance histograms were produced from  $\log_{10}(\frac{I}{V-C_0})$  values calculated for every data point.

## Supporting Information

Supporting Information is available from the Wiley Online Library or from the author.

## Acknowledgements

The authors thank the Ministry of Education of Saudi Arabia and King Abdulaziz University for financial support for H.A.G. (Grant: KAU1526). J.G.H. thanks the UK Engineering and Physical Sciences Research Council for financial support (via grants EP/R003823/1, EP/R511560/1 and EP/K03099X/1), and the UK Biotechnology and Biological Sciences Research Council for financial support (via grant BB/L0137971/1) and the UK Royal Society for financial support (via grant: RG160449). F.H.S. and J.E. acknowledge funding by the Deutsche Forschungsgemeinschaft (Project B05 within the Sonderforschungsbereich SFB/TRR 234 "Catalight", project ID: 364549901). The authors thank the British Council and Egyptian Ministry of Higher Education Newton-Mosharafa Ph.D. Programme for a studentship to support H.A.M.A. (Grant Reference: NMM28/20). E.P. and J.G.H. acknowledge funding from TUBITAK, via the TUBITAK-BIDEB 2219-International Postdoctoral Research Fellowship Program (Grant Reference: 1059B191900691). The authors thank Rob Short at the University of Sheffield for insightful discussions about XPS.

## Conflict of Interest

The authors declare no conflict of interest. The funders had no role in the design of the study; in the collection, analyses, or interpretation of data; in the writing of the manuscript, or in the decision to publish the results.

## Author Contributions

K.V., A.M.T., and J.G.H. conceptualized the work; all authors worked on methodology; all authors worked on formal analysis; H.A.G., J.E., S.H.,

A.J.R., L.M., H.A.M.A., E.P., S.J.B., N.R.H., and V.C. investigated the work; H.A.G. and J.G.H. wrote the original draft; all authors reviewed and edited the work; F.H.S., B.J.R., A.M.T., and J.G.H. supervised the work; A.M.T. and J.G.H. worked on project administration; F.H.S., B.J.R., K.V., A.M.T., and J.G.H. worked on funding acquisition. All authors read and agreed to the published version of the manuscript.

## Data Availability Statement

The data that support the findings of this study are available from the corresponding author upon reasonable request.

## Keywords

conjugated polymers, doping, melanins, organic electronics, phenols

Received: January 31, 2023

Revised: May 21, 2023

Published online:

- [1] P. Delparastan, K. G. Malollari, H. Lee, P. B. Messersmith, *Angew. Chem., Int. Ed.* **2019**, *58*, 1077.
- [2] F. Solano, *New J. Sci.* **2014**, *2014*, 498276.
- [3] L. Klosterman, J. K. Riley, C. J. Bettinger, *Langmuir* **2015**, *31*, 3451.
- [4] C. Grieco, F. R. Kohl, A. T. Hanes, B. Kohler, *Nat. Commun.* **2020**, *11*, 4569.
- [5] W. Cao, X. Zhou, N. C. McCallum, Z. Hu, Q. Z. Ni, U. Kapoor, C. M. Heil, K. S. Cay, T. Zand, A. J. Mantanona, A. Jayaraman, A. Dhinojwala, D. D. Deheyn, M. D. Shawkey, M. D. Burkart, J. D. Rinehart, N. C. Gianneschi, *J. Am. Chem. Soc.* **2021**, *143*, 2622.
- [6] H. A. Galeb, E. L. Wilkinson, A. F. Stowell, H. Lin, S. T. Murphy, P. L. Martin-Hirsch, R. L. Mort, A. M. Taylor, J. G. Hardy, *Global Challenges* **2021**, *5*, 2000102.
- [7] M. Xiao, M. D. Shawkey, A. Dhinojwala, *Adv. Opt. Mater.* **2020**, *8*, 2000932.
- [8] A. B. Mostert, *Polymers* **2021**, *13*, 1670.
- [9] J. Park, H. Moon, S. Hong, *Biomater. Res.* **2019**, *23*, 24.
- [10] M. Caldas, A. C. Santos, F. Veiga, R. Rebelo, R. L. Reis, V. M. Correlo, *Acta Biomater.* **2020**, *105*, 26.
- [11] L. Huang, M. Liu, H. Huang, Y. Wen, X. Zhang, Y. Wei, *Biomacromolecules* **2018**, *19*, 1858.
- [12] S. Ito, K. Wakamatsu, *Pigm. Cell Res.* **2003**, *16*, 523.
- [13] S. Ito, K. Wakamatsu, *Photochem. Photobiol.* **2008**, *84*, 582.
- [14] J. D. Simon, D. N. Peles, *Acc. Chem. Res.* **2010**, *43*, 1452.
- [15] V. J. Hearing, *J. Invest. Dermatol.* **2011**, *131*, E8.
- [16] J. A. Swift, *Int. J. Cosmet. Sci.* **2009**, *31*, 143.
- [17] Q. Z. Ni, B. N. Sierra, J. J. La Clair, M. D. Burkart, *Chem. Sci.* **2020**, *11*, 7836.
- [18] S. Ito, S. Miyake, S. Maruyama, I. Suzuki, S. Commo, Y. Nakanishi, K. Wakamatsu, *Pigm. Cell Melanoma Res.* **2018**, *31*, 393.
- [19] S. Ito, K. Wakamatsu, T. Sarna, *Photochem. Photobiol.* **2018**, *94*, 409.
- [20] B. Watt, G. van Niel, G. Raposo, M. S. Marks, *Pigm. Cell Melanoma Res.* **2013**, *26*, 300.
- [21] C. Bissig, L. Rochin, G. Van Niel, *Int. J. Mol. Sci.* **2016**, *17*, 1438.
- [22] G. Nasiri, N. Azarpira, A. Alizadeh, S. Goshtasbi, L. Tayebi, *Stem Cell Res. Ther.* **2020**, *11*, 421.
- [23] F. A. Zucca, A. Capuccini, C. Bellei, M. Sarna, T. Sarna, E. Monzani, L. Casella, L. Zecca, *IUBMB Life* **2023**, *75*, 55.
- [24] D. E. Korzhevskii, O. V. Kirik, V. V. Guselnikova, D. L. Tsyba, E. A. Fedorova, I. P. Grigorev, *Eur. J. Histochem.* **2021**, *65*, 3283.
- [25] E. Camacho, R. Vij, C. Chrissian, R. Prados-Rosales, D. Gil, R. N. O'meally, R. J. B. Cordero, R. N. Cole, J. M. McCaffery, R. E. Stark, A. Casadevall, *J. Biol. Chem.* **2019**, *294*, 10471.

- [26] N. E.-A. El-Naggar, W. I. A. Saber, *Polymers* **2022**, *14*, 1339.
- [27] A. Y. Glagoleva, O. Y. Shoeva, E. K. Khlestkina, *Front. Plant Sci.* **2020**, *11*, 770.
- [28] K. Tajima, D. Yamanaka, K.-I. Ishibashi, Y. Adachi, N. Ohno, *FEBS Open Bio* **2019**, *9*, 791.
- [29] F. Solano, *Int. J. Mol. Sci.* **2017**, *18*, 1561.
- [30] S. Park, C. Lee, J. Lee, S. Jung, K.-Y. Choi, *Biotechnol. Bioprocess Eng.* **2020**, *25*, 646.
- [31] F. Scognamiglio, A. Travan, G. Turco, M. Borgogna, E. Marsich, M. Pasqua, S. Paoletti, I. Donati, *Colloids Surf., B* **2017**, *155*, 553.
- [32] H. Feinberg, T. W. Hanks, *Polym. Int.* **2022**, *71*, 578.
- [33] H. A. Lee, E. Park, H. Lee, *Adv. Mater.* **2020**, *32*, 1907505.
- [34] S. H. Hong, S. Hong, M.-H. Ryou, J. W. Choi, S. M. Kang, H. Lee, *Adv. Mater. Interfaces* **2016**, *3*, 1500857.
- [35] M. Lee, S.-H. Lee, I.-K. Oh, H. Lee, *Small* **2017**, *13*, 1600443.
- [36] S. Kim, L. K. Jang, M. Jang, S. Lee, J. G. Hardy, J. Y. Lee, *ACS Appl. Mater. Interfaces* **2018**, *10*, 33032.
- [37] W. Cao, X. Zhou, N. C. McCallum, Z. Hu, Q. Z. Ni, U. Kapoor, C. M. Heil, K. S. Cay, T. Zand, A. J. Mantanona, A. Jayaraman, A. Dhinojwala, D. D. Deheyn, M. D. Shawkey, M. D. Burkart, J. D. Rinehart, N. C. Gianneschi, *J. Am. Chem. Soc.* **2021**, *143*, 2622.
- [38] A. A. Putnam, J. J. Wilker, *Soft Matter* **2021**, *17*, 1999.
- [39] M. Dunbar, S. Ketten, *Macromolecules* **2020**, *53*, 9397.
- [40] X. Hu, Z. Li, Z. Yang, F. Zhu, W. Zhao, G. Duan, Y. Li, *ACS Macro Lett.* **2022**, *11*, 251.
- [41] A. Moliton, R. C. Hiorns, *Polym. Int.* **2004**, *53*, 1397.
- [42] S. Kobayashi, *J. Polym. Sci., Part A: Polym. Chem.* **1999**, *37*, 3041.
- [43] N. Aktas, N. Sahiner, Ö. Kantoglu, B. Salih, A. Tanyolaç, *J. Polym. Environ.* **2003**, *11*, 123.
- [44] S. Dubey, D. Singh, R. A. Misra, *Enzyme Microb. Technol.* **1998**, *23*, 432.
- [45] N. Li, H.-B. Wang, L. Thia, J.-Y. Wang, X. Wang, *Analyst* **2015**, *140*, 449.
- [46] F. Li, Y. Yu, Q. Wang, J. Yuan, P. Wang, X. Fan, *Enzyme Microb. Technol.* **2018**, *119*, 58.
- [47] H. A. Galeb, A. Lamantia, A. Robson, K. König, J. Eichhorn, S. J. Baldock, M. D. Ashton, J. V. Baum, R. L. Mort, B. J. Robinson, F. H. Schacher, V. Chechik, A. M. Taylor, J. G. Hardy, *Macromol. Chem. Phys.* **2022**, *223*, 2100489.
- [48] R. J. Waltman, J. Bargon, *Can. J. Chem.* **1986**, *64*, 76.
- [49] H. Ma, Y. Chen, X. Li, B. Li, *Adv. Funct. Mater.* **2021**, *31*, 2101861.
- [50] M. R. J. Scherer, in *Double-Gyroid-Structured Functional Materials: Synthesis and Applications* (Ed. M. R. J. Scherer), Springer International Publishing, Heidelberg **2013**, pp. 135.
- [51] Q. Zhang, H. Dong, W. Hu, *J. Mater. Chem. C* **2018**, *6*, 10672.
- [52] R. Pourghobadi, D. Nematollahi, M. R. Baezzat, S. Alizadeh, H. Goljani, *J. Electroanal. Chem.* **2020**, *866*, 114180.
- [53] E. Voisin, V. E. Williams, *Macromolecules* **2008**, *41*, 2994.
- [54] K. Yong, M. Shao-Lin, *Chin. J. Chem.* **2003**, *21*, 630.
- [55] S. Li, H. Wang, M. Young, F. Xu, G. Cheng, H. Cong, *Langmuir* **2019**, *35*, 1119.
- [56] F. Lorquin, P. Piccerelle, C. Orneto, M. Robin, J. Lorquin, *J. Ind Microbiol Biotechnol* **2022**, *49*, kuac013.
- [57] B. Stöckle, D. Y. W. Ng, C. Meier, T. Paust, F. Bischoff, T. Diemant, R. J. Behm, K. E. Gottschalk, U. Ziener, T. Weil, *Macromol. Symp.* **2014**, *346*, 73.
- [58] S. Kobayashi, H. Higashimura, *Prog. Polym. Sci.* **2003**, *28*, 1015.
- [59] S. Kobayashi, S.-i. Shoda, H. Uyama, in *Polymer Synthesis/Polymer Engineering*, Springer, Berlin Heidelberg, Berlin, Heidelberg **1995**, pp. 1–30.
- [60] A. C. Ferrari, F. Bonaccorso, V. Fal'ko, K. S. Novoselov, S. Roche, P. Bøggild, S. Borini, F. H. L. Koppens, V. Palermo, N. Pugno, J. A. Garrido, R. Sordan, A. Bianco, L. Ballerini, M. Prato, E. Lidorikis, J. Kivioja, C. Marinelli, T. Ryhänen, A. Morpurgo, J. N. Coleman, V. Nicolosi, L. Colombo, A. Fert, M. Garcia-Hernandez, A. Bachtold, G. F. Schneider, F. Guinea, C. Dekker, M. Barbone, et al., *Nanoscale* **2015**, *7*, 4598.
- [61] K. Saito, G. Sun, H. Nishide, *Green Chem. Lett. Rev.* **2007**, *1*, 47.
- [62] L. W. Flanagan, C. L. Mcadams, W. D. Hinsberg, I. C. Sanchez, C. G. Willson, *Macromolecules* **1999**, *32*, 5337.
- [63] M. Nicolai, G. Gonçalves, F. Natalio, M. Humanes, *J. Inorg. Biochem.* **2011**, *105*, 887.
- [64] S. N. Dezidério, C. A. Brunello, M. I. N. Da Silva, M. A. Cotta, C. F. O. Graeff, *J. Non-Cryst. Solids* **2004**, *338*, 634.
- [65] V. Capozzi, G. Perna, P. Carmone, A. Gallone, M. Lastella, E. Mezzenga, G. Quartucci, M. Ambrico, V. Augelli, P. F. Biagi, T. Ligonzo, A. Minafra, L. Schiavulli, M. Pallara, R. Cicero, *Thin Solid Films* **2006**, *511*, 362.
- [66] G. Khouqeer, M. Alghrably, N. Madkhali, M. Dhahri, M. Jaremko, A.-H. Emwas, *Nano Sel.* **2022**, *3*, 1598.
- [67] B. Simonovic, V. Vucelic, A. Hadzi-Pavlovic, K. Stepien, T. Wilczok, D. Vucelic, *J. Therm. Anal. Calorim.* **1990**, *36*, 2475.
- [68] G. Beamson, D. Briggs, *Physics* **1992**, 92946956.
- [69] J. Moulder, W. Stickle, P. Sobol, K. Bomben, G. Muilenberg, *Handbook of X-ray Photoelectron Spectroscopy*, PerkinElmer, Inc., Waltham, MA, USA **1992**.
- [70] A. Büngeler, B. Hämisch, O. I. Strube, *Int. J. Mol. Sci.* **2017**, *18*, 1901.
- [71] X. Ma, Z. Sun, W. Su, Z. Yi, X. Cui, B. Guo, X. Li, *J. Mater. Chem. B* **2018**, *6*, 3811.
- [72] L. Klosterman, C. Bettinger, *Int. J. Mol. Sci.* **2017**, *18*, 14.
- [73] L. Hong, J. D. Simon, *J. Phys. Chem. B* **2007**, *111*, 7938.
- [74] Y. J. Kim, W. Wu, S.-E. Chun, J. F. Whitacre, C. J. Bettinger, *Proc. Natl. Acad. Sci. U. S. A.* **2013**, *110*, 20912.
- [75] P. Kumar, E. Di Mauro, S. Zhang, A. Pezzella, F. Soavi, C. Santato, F. Ciccoira, *J. Mater. Chem. C* **2016**, *4*, 9516.
- [76] L. Yang, X. Guo, Z. Jin, W. Guo, G. Duan, X. Liu, Y. Li, *Nano Today* **2021**, *37*, 101075.
- [77] A. Gouda, A. Masson, M. Hoseinizadeh, F. Soavi, C. Santato, *Commun. Chem.* **2022**, *5*, 98.
- [78] B. Bilinska, *Spectrochim. Acta, Part A* **1996**, *52*, 1157.
- [79] M. Al Khatib, J. Costa, D. Spinelli, E. Capecci, R. Saladino, M. C. Baratto, R. Pogni, *Int. J. Mol. Sci.* **2021**, *22*, 1739.
- [80] H. Wei, J. Ren, B. Han, L. Xu, L. Han, L. Jia, *Colloids Surf., B* **2013**, *110*, 22.
- [81] Z.-Y. Xi, Y.-Y. Xu, L.-P. Zhu, Y. Wang, B.-K. Zhu, *J. Membr. Sci.* **2009**, *327*, 244.
- [82] J. Stainsack, A. S. Mangrich, C. M. B. F. Maia, V. G. Machado, J. C. P. Dos Santos, S. Nakagaki, *Inorg. Chim. Acta* **2003**, *356*, 243.
- [83] S. Paim, L. F. Linhares, A. S. Mangrich, J. P. Martin, *Biol. Fertil. Soils* **1990**, *10*, 72.
- [84] T. Sarna, H. M. Swartz, A. Zadlo, *Appl. Magn. Reson.* **2022**, *53*, 105.
- [85] C. C. Felix, J. S. Hyde, T. Sarna, R. C. Sealy, *J. Am. Chem. Soc.* **1978**, *100*, 3922.
- [86] J. Szweczyk, D. Aguilar-Ferrer, E. Coy, *Eur. Polym. J.* **2022**, *174*, 111346.
- [87] P. Meredith, T. Sarna, *Pigment Cell Res* **2006**, *19*, 572.
- [88] E. Vahidzadeh, A. P. Kalra, K. Shankar, *Biosens. Bioelectron.* **2018**, *122*, 127.
- [89] J. V. Paulin, C. F. O. Graeff, *J. Mater. Chem. C* **2021**, *9*, 14514.
- [90] K. Namsheer, C. S. Rout, *RSC Adv.* **2021**, *11*, 5659.
- [91] M. Bajpai, R. Srivastava, R. Dhar, R. Tiwari, *J. Mater. Sci. Mater. Med.* **2016**, *2016*, 1.
- [92] W. Han, M. He, M. Byun, B. Li, Z. Lin, *Angew. Chem., Int. Ed.* **2013**, *52*, 2564.
- [93] A. O. Patil, Y. Ikenoue, N. Basescu, N. Colaneri, J. Chen, F. Wudl, A. J. Heeger, *Synth. Met.* **1987**, *20*, 151.



- [94] D. A. Lukyanov, A. A. Vereshchagin, A. V. Soloviova, O. V. Grigorova, P. S. Vlasov, O. V. Levin, *ACS Appl. Energy Mater.* **2021**, *4*, 5070.
- [95] C. Beaumont, J. Turgeon, M. Idir, D. Neusser, R. Lapointe, S. Caron, W. Dupont, D. D'astous, S. Shamsuddin, S. Hamza, É. Landry, S. Ludwigs, M. Leclerc, *Macromolecules* **2021**, *54*, 5464.
- [96] I. Imae, K. Krukiewicz, *Bioelectrochemistry* **2022**, *146*, 108127.
- [97] C. Phornphutkul, W. J. Introne, M. B. Perry, I. Bernardini, M. D. Murphey, D. L. Fitzpatrick, P. D. Anderson, M. Huizing, Y. Anikster, L. H. Gerber, W. A. Gahl, *N. Engl. J. Med.* **2002**, *347*, 2111.
- [98] J. B. Mistry, M. Bukhari, A. M. Taylor, *Rare Dis.* **2013**, *1*, e27475.
- [99] A. Bernini, E. Petricci, A. Atrei, M. C. Baratto, F. Manetti, A. Santucci, *Sci. Rep.* **2021**, *11*, 22562.
- [100] A. M. Taylor, K. P. Vercruysse, *JIMD Reports*, Vol. 35, Springer, Berlin **2017**, pp. 79.
- [101] M. d'Ischia, A. Napolitano, A. Pezzella, P. Meredith, M. J. Buehler, *Angew. Chem., Int. Ed.* **2020**, *59*, 11196.
- [102] M. d'Ischia, A. Napolitano, A. Pezzella, P. Meredith, T. Sarna, *Angew. Chem., Int. Ed.* **2009**, *48*, 3914.
- [103] M. d'Ischia, *Int. J. Mol. Sci.* **2018**, *19*, 228.
- [104] V. Ball, *Biomimetics* **2017**, *2*, 12.
- [105] M. Ambrico, P. F. Ambrico, T. Ligonzo, A. Cardone, S. R. Cicco, M. D'ischia, G. M. Farinola, *J. Mater. Chem. C* **2015**, *3*, 6413.
- [106] J. H. Ryu, P. B. Messersmith, H. Lee, *ACS Appl. Mater. Interfaces* **2018**, *10*, 7523.
- [107] EasySpin, <https://easyspin.org/>.